A tribological assessment of 17-4PH stainless steel manufactured by binder jetting

L. Fabiocchi, M. Mariani, A. Lucchini Huspek, M. Pozzi, M. Bestetti, S. Graziosi, N. Lecis

This study presents an investigation into the mechanical and tribological properties of binder jetting 17-4PH (AISI 630) stainless steel, with a focus on the interplay between surface finishing and thermal treatments. A subset of samples was superficially treated with a Low Energy High Current Electron Beam, varying the energy density (J/cm2), whereas another set of specimens was thermally treated by solution annealing and aging (H900). Experimental analyses included visual inspection, roughness measurements, microhardness testing, and wear tests.

Optical microscopy provided insights into the surface morphology and treatment-dependent defects. Roughness measurements quantified the surface texture alterations, while microhardness tests determined the effect of treatments on the mechanical properties of the material. Tribological tests evaluated the sample wear resistance and the material behaviour during sliding. Analysis of wear behaviour correlated with specific surface finishing or thermal treatments aimed to distinguish their effects on friction coefficients and wear track morphology across samples.

KEYWORDS: STAINLESS STEEL 17-4PH, BINDER JETTING, LOW ENERGY HIGH CURRENT ELECTRON BEAM, TRIBOLOG, SURFACE FINISHING

INTRODUCTION

Additive manufacturing (AM) of stainless steels is rapidly developing thanks to the ability to achieve complex designs effortlessly. This capability is relevant in industrial sectors where limited-scale production coupled with customization is demanded, such as the biomedical field: prostheses as well as surgical instruments tailored to the users' needs, would greatly benefit from enhancement in terms of dimensional accuracy, functionality, and weight reduction. Among different techniques, binder jetting (BJT) is emerging owing to the possibility of using specific alloys employed in this sector (e.g. stainless steels, titanium, CoCrMo). This process yields final microstructures akin to those produced through conventional manufacturing processes, especially those associated with sinter-based approaches. When utilized for 17-4 PH stainless steel (AISI 630), a martensitic precipitation-hardening alloy, BJT provides notable benefits in terms of scalability and cost reduction. The technique works by depositing a binder onto layers of metal powder, forming a green part that is later sintered to achieve the desired mechanical properties. For 17-4 PH steel, crucial post-processing steps, including debinding, sintering, and heat treatments, are necessary to achieve the optimal mechanical characteristics such

L. Fabiocchi, M. Mariani, S. Graziosi, N. Lecis
Dipartimento di Meccanica, Politecnico di Milano

A. Lucchini Huspek, M. Bestetti
Dipartimento di Chimica, Materiali e Ingegneria Chimica "Giulio Natta", Politecnico di Milano

M. Pozzi
Dipartimento di Chimica, Materiali e Ingegneria Chimica "Giulio Natta", Politecnico di Milano – Rösler Italiana s.r.l.

lorenza.fabiocchi@polimi.it

as strength, hardness, and corrosion resistance. This approach is opening new routes for the production of high-performance components with complex designs even in the case of materials with low machinability, such as 17-4PH, that hinders the manufacturing of geometries without the aid of expensive tools and processes [1].

The surface characteristics of binder jetted components are critical to their performance, particularly in applications requiring high precision and durability in demanding environments. Key surface properties such as roughness, porosity, and microstructure significantly influence the wear resistance, fatigue life, and corrosion behaviour of these parts. Since BJT often produces components with relatively high surface roughness compared to machining subtractive manufacturing, additional finishing processes like polishing, machining, or coating are often required to enhance the surface quality. Moreover, the surface characteristics can have a profound impact on the mechanical performance, especially in applications that demand high reliability and precision. Therefore, optimizing surface properties is essential to ensure the functional success of binder jetted components [2,3].

Low Energy High Current Electron Beam (LEHCEB) technology has emerged as a viable surface finishing solution for binder jetted components, particularly for 17-4 PH stainless steel parts. This technique uses short (2.5 μs), intense pulses (1 – 6 J/cm^2) of electron beams to rapidly melt and modify a thin surface layer (~10 μm), resulting in a smoother, more refined finish. LEHCEB reduces surface roughness, minimizes porosity, and improves microstructural uniformity which in turn enhances mechanical and tribological properties such as hardness and wear resistance. Additionally, this treatment can improve corrosion resistance by refining the grain structure and eliminating surface imperfections. Since LEHCEB does not modify the bulk properties of the material, it is an efficient and precise technique for improving surface quality in binder jetted parts, especially those used in high-performance applications. Nonetheless, it should be considered that the heat and the residual stresses generated by the process may induce microstructural changes in the sub-surface regions, especially in a temperature-sensitive alloy. Indeed, given the high copper concentrations in 17-4PH steel, the material properties can be widely adjusted by thermal aging through precipitation hardening treatments: copper precipitates form within the supersaturated martensite grains, at first as coherent BCC clusters, then they grow into incoherent FCC phases. The nucleation of the Cu precipitates, as well as their coalescence, depends on the aging treatment conditions [4,5].

This study aims to determine the effect of LEHCEB treatment on the microstructural properties of the surface region and the tribological performance of 17-4PH steel components produced by BJT. The effectiveness of this surface finishing is assessed by comparison with the bulk and surface microstructural properties and wear resistance of as-sintered and thermally aged components.

MATERIALS AND METHODS

Sample preparation

The samples were manufactured with a Desktop Metal Shop System employing a pre-alloyed gas atomized powder with a D90 of 50 μm and a layer thickness of 75 μm. A commercial aqueous-based binder containing polyethylene glycol monomers was used in this study.

After the BJT process, the powder bed was cured in a natural convection air furnace at 180 °C for 6 hours to polymerize the binder and strengthen the green parts. The debinding and sintering treatments were performed in a single cycle in a slightly reducing atmosphere (97% Ar / 3% H_2) to remove most of the organic binder and achieve a satisfactory densification of the material, while avoiding the oxidation of the components surface [6]. The samples were cooled in the furnace at a low rate until room temperature was achieved.

After sintering, a conventional H900 aging treatment at 480 °C for 1 hour was applied to the specimens, after an initial solution annealing cycle at 1050 °C for 1 hour. To avoid the oxidation of the surface, both treatments were realized in sequence in a low vacuum atmosphere with N_2-assisted rapid cooling.

The Low-Energy High-Current Electron Beam (LEHCEB) surface was performed in a RITM-SP facility. Irradiation pressure was set at 1.8·10-4 torr with Ar as background gas. Two different accelerating voltage, 20 and 30 kV, were investigated, corresponding to an energy density value of 2.5 and 4.6 J/cm^2, respectively. The applied number of pulses was 20 with a repetition frequency of 0.2 Hz. After LEHCEB irradiation samples were cooled down within

the vacuum chamber in saturated Ar environment for 45 minutes to avoid oxidation phenomena.

Components characterization

Micrographies of the samples were obtained after standard metallographic procedures and etching (Kalling I reagent). Microstructural analysis was conducted by scanning electron microscopy (SEM) equipped with energy dispersive x-ray spectroscopy (EDX). Roughness measurements were performed using a contact profilometer (Formtracer Avant, Mitutoyo) repeating the test 5 times with a measuring length of 4.8 mm and a 0.8 mm cut-off, according to the ISO 4287 standard. Hardness was assessed by a Vickers indentation testing with an applied load of 300 gf for 15 seconds. Tribological assessment was performed by using an RTEC tribometer in the linear reciprocating pin on disk configuration. An alumina ball was used as opponent material and a load of 2 N was chosen for all tests. The frequency of the reciprocating linear movement was set at 10 Hz while the duration of the test was fixed at 10 minutes.

RESULTS

Bulk microstructure

Debinding and sintering involve phase transformations; the most significant occur during cooling from the sintering temperature. Above 1300 °C the microstructure is composed of austenite and a fraction of δ ferrite, that can dissolve a smaller fraction of copper. The initial rapid cooling from high temperature preserves the δ ferrite formed within the microstructure, identified by the fraction rich in ferritizing elements such as chromium (Figure 1) [7,8]. After the thermal gradient stabilization below 800 °C, low cooling rates allow the nucleation of copper precipitates and their growth into enlarged FCC phases, mainly within the ferrite and predominantly at grain boundaries among parent austenitic grains, as visible in Figure 1. The formation of copper precipitates occurs to a greater extent in the ferritic phase during cooling, due to the lower solubility of copper in δ- compared to γ-phase, and the larger diffusivity in the BCC lattice allows a faster coalescence of copper rich-phases (identified by orange circles in Figure 1). The segregation of precipitates at grain boundaries is due to the diffusion of austenitizing elements from ferrite to austenite during cooling and their preferential nucleation at the interphase interface, where growth leads to the transition from a coherent BCC structure to an incoherent FCC structure that is more stable. Precipitation in the main phase is initially limited by the high solubility of copper in austenite and, after martensitic transformation, by low temperatures at this stage (M_s < 300 °C). In addition, niobium carbides (identified by orange circles in Figure 1) can be identified by high-magnification EDX analysis both within the ferrite and at the grain boundaries of the martensite.

Solution annealing eliminates copper precipitates by resolubilizing them in austenite at high temperature, thus allowing its controlled precipitation in the following aging processes. The metallographies in Figure 2 reveal that niobium carbides (purple circles) can still be found along the grain boundaries of martensite regardless of the thermal treatment performed, given its stability well above 1100 °C. Copper-rich phases (pink circles) can be detected along the grain boundaries and within the ferrite of the H900 specimen, but the extent of their presence is largely limited with respect to the as-sintered condition.

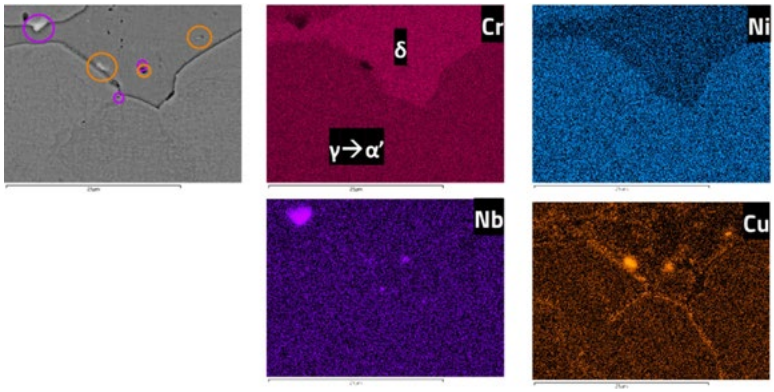

Fig.1 - EDX maps of the main alloying elements of an as-sintered specimen.

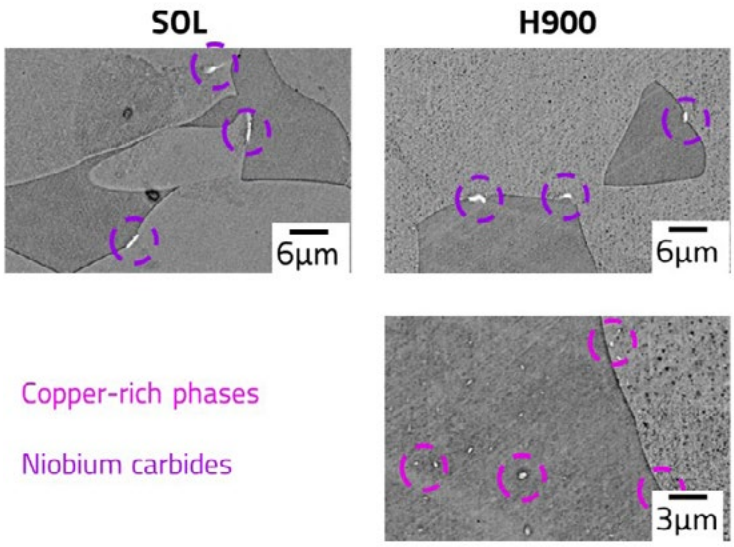

Fig.2 - SEM micrographs of the solution annealed and aged (H900) specimens, with the identification of niobium carbides (purple) and copper-rich phases (pink).

It can be observed in Figure 3 that the H900 treatment was able to produce a slight increase in the average hardness value with respect to the as-sintered condition, which is correlated to the formation of fine coherent copper precipitates after solution annealing, especially in the copper-rich martensite. Nonetheless, the standard deviation of the H900 condition is extremely large and the measured values partially overlap with those obtained for the as-sintered condition. It can be expected that in many cases the indentation was influenced by the presence of porosity and δ ferrite which are softer than martensite, especially after precipitation hardening. One of the surface treated components was analysed as well to determine whether the LEHCEB process would be able to affect the core region of the component: it can be observed that the hardness measured is comparable to that of the as-sintered condition, thus confirming that the surface finishing does not affect the bulk properties of the material.

The Vickers values were converted to Rockwell C hardness values to allow a preliminary comparison with the hardness requested by the ASTM A564/A564M - 19a standard for the H900 aged specimens produced by conventional manufacturing. It can be observed that the treated component does not satisfy the requirement of the standard, at least in terms of average value. Performing macroscopic indentations may produce different results with respect to conversion from Vickers values, although it should be considered that the presence of porosity and δ ferrite in that case would still be influential because macroscopic indentations could not avoid these defects.

The poor performance of H900 specimens could suggest that nitrogen-assisted cooling in furnace is not as effective as water quenching or air cooling in the whole range of temperature. The employed procedure increases the cooling rate at high temperatures with respect to furnace cooling, but it cannot maintain such rate until room temperature is achieved. Slower rates could favour the occurrence of undesired nucleation and growth of precipitates, and excessive tempering of the martensite, especially after solution annealing at high temperature, with detrimental effects on hardness.

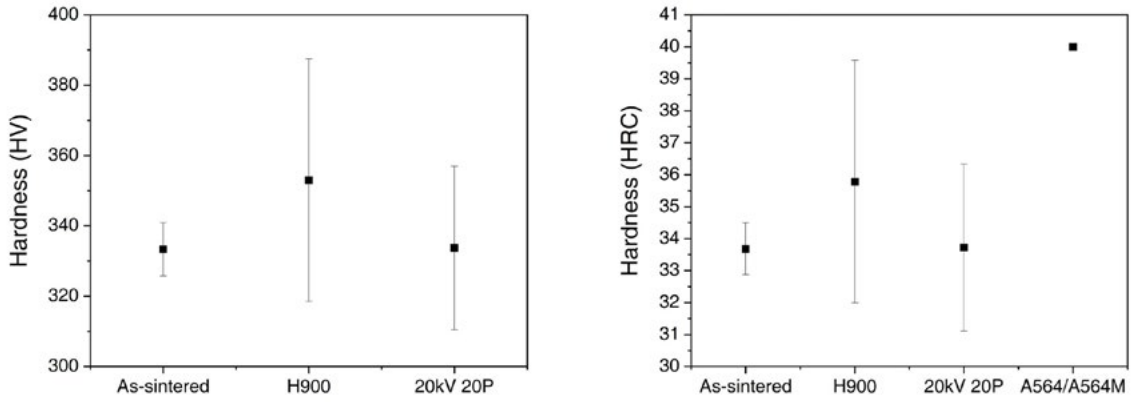

Fig.3 - Vickers (left) and Rockwell C (right) hardness values.

Surface microstructure

As can be seen from Figure 4, the LEHCEB treatment mitigates the surface inhomogeneity of the as-sintered specimens, which is typically influenced by the particles size and by the layerwise deposition method. The surface average roughness (Ra) is reduced by increasing the voltage of the electron beam from 20 kV to 30 kV, as verified by the measurement performed on the y direction parallel to the wear track on the samples, shown in Figure 5. In addition to the average roughness value decrease, also the standard deviation of the measurements on the surface-treated components is reduced, owing to the complete filling of the surface valleys generated by residual porosity, mostly in correspondence with the interlayer regions. These areas are known to be preferentially affected by the presence of open porosity near the surface, due to the additional macroscopic voids generated by the removal of the organic binder during the preliminary debinding process [9].

The cross sections of the surface treated samples were analysed to determine the thickness of the melted layer by the LEHCEB and to evaluate variations in the type of microstructural features. As can be seen in Figure 6, the accelerating voltage of the electron beam has a great influence on the resulting surface: the treated layer of the 20 kV sample is extremely thin (< 1 μm) and not as homogeneous as the one of the 30 kV samples, whose thickness reaches about 4 μm. It can be observed, especially in the 30 kV specimen, that the treated surfaces have a uniform microstructure constituted by martensitic grains, which are finer than those within the bulk volume that extend for tens of micrometres. It can be noted as well that δ phase regions seem to be completely absent in correspondence with martensitic grains and almost completely removed where this kind of ferrite was reaching the surface in the as-sintered specimen. Therefore, the fusion of the surface material and the subsequent rapid cooling does not allow for the nucleation of ferritic grains, but rather the formation of austenite followed by the martensitic transformation at low temperature.

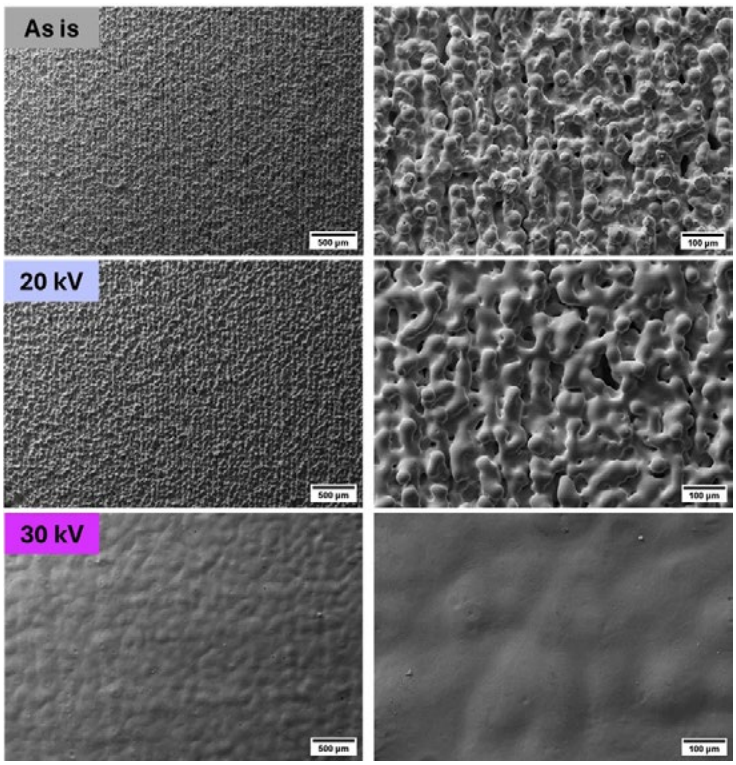

Fig.4 - SEM images of the surface morphology of as-sintered and surface treated (LEHCEB) samples at 20 kV and 30 kV.

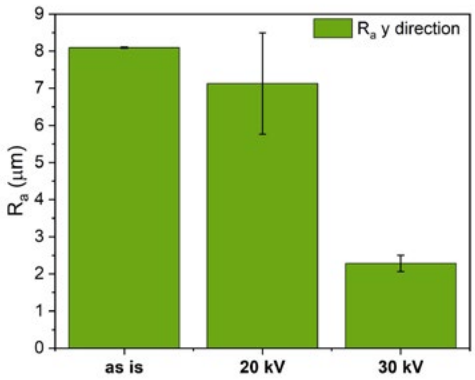

Fig.5 - Mean roughness values measured in the y direction of the samples surface.

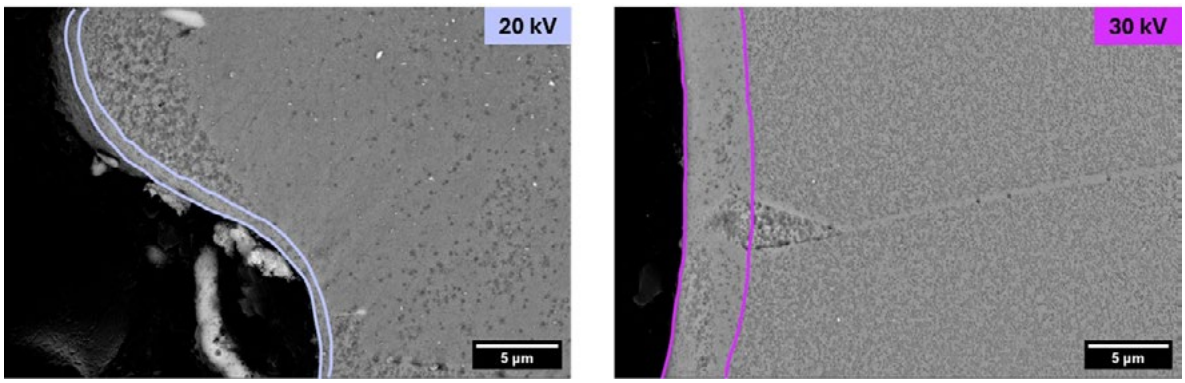

Fig.6 - SEM micrographs of the melted surface region highlighted between the light purple lines for 20kV and fuchsia lines for 30 kV.

Surface tribological performance

From Figure 7, it can be observed that all the specimens display the achievement of a stable coefficient of friction (COF) after an initial transition. Nonetheless, the nature and the duration of the low friction region vary according to the selected parameters for the treatment. Indeed, the as-sintered specimen experiences an immediate and continuous transition toward an average COF above 0.9. The H900 aged material progressively stabilizes at a friction coefficient value lower than 0.6, thanks to the hardening effect of copper precipitation in the martensitic grains. The surface treated samples (light purple and fuchsia lines in Figure 7) present two distinguishable regions of the curve connected by a sharp transition: the first with a stable low friction coefficient at about 0.1 and the second with a COF in the 0.4-0.7 range. The stabilization at low friction value is evident for the sample treated at 30 kV, whereas it is interrupted rapidly for that obtained at 20 kV. The characteristic behaviour of the modified surfaces can be explained by the abrupt change of the microstructural and mechanical properties of the material when the complete wear of the molten layer, formed during the electron beam treatment, is achieved. This hypothesis is confirmed by the visible shift of the second region in the sample superficially treated with a beam acceleration of 30 kV compared to the one treated with a lower voltage. In fact, the tempered martensitic layer of the 20 kV pulses is thinner compared to that of the 30 kV, leading to an earlier consumption under equal testing conditions. As the pure martensitic surface layer is consumed and the coupling with the alumina ball changes to the sub-surface region, the wear resistance is reduced and the friction increases owing to the presence of ferrite and martensite with a different thermal history.

In both cases the friction coefficient in the second region stabilizes at a lower value with respect to the as-sintered sample (black line in Figure 7), although the sub-surface material should not be directly affected by the LEHCPEB treatment. In fact, the friction behaviour seems comparable to that of the H900 sample (red line in Figure 7), whose improved performance is associated with the formation of coherent precipitate in the martensitic matrix. Therefore, the difference between the COF of the as-sintered sample and the second region of the superficially treated samples is hypnotized to be linked to the formation of a heat affected zone (HAZ) in the sub-surface region, which modifies the tribological behaviour of these samples even after the consumption of the molten layer.

The roughness of treated samples, together with the thickness of the quenched layer, plays a critical role in the wear track morphology (Figure 8). The surface treated at 20 kV has a broader and more spread track compared to the one at 30 kV, even if the roughness is higher. The as-sintered specimen track is more distributed due to a higher plastic deformation caused by the lower hardness of the material, even if the roughness is comparable to the one of the superficially treated at 20 kV. Finally, the wear track of the sample treated at 30 kV is minimized owing to the reduced wear rate in correspondence with the low COF region that lasted for more than half of the test duration.

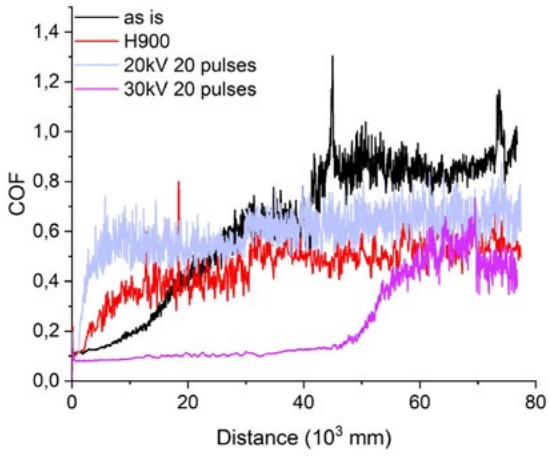

Fig.7 - Coefficient of friction measured for surface treated (light purple and fuchsia), thermally aged (red) and as-sintered (black) samples.

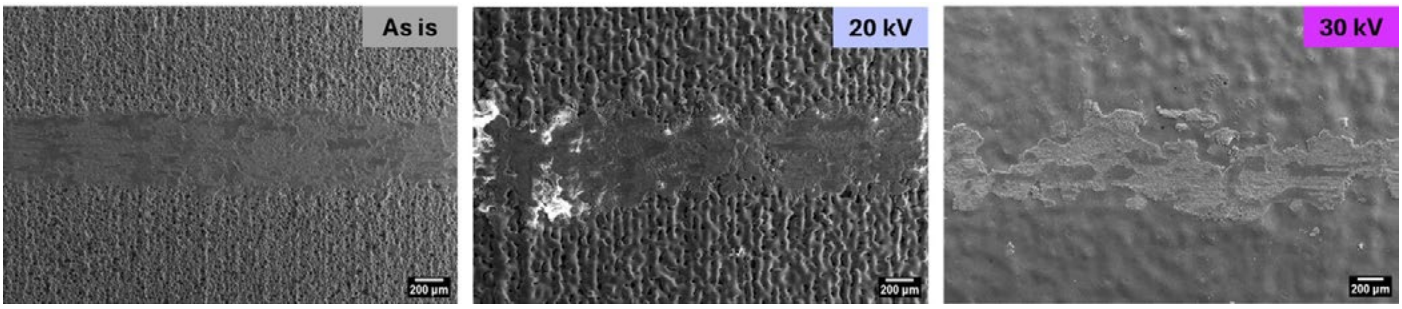

Fig.8 - SEM images of the wear track morphology of samples at the as-sintered state (left), surface treated at 20 (centre) and 30 kV (right).

CONCLUSIONS

The analysis of the bulk and surface microstructures, as well as the surface tribological performance, provides several insights into the behaviour of the material under different processing conditions.

The cooling process following sintering preserves δ ferrite and promotes the nucleation and growth of copper precipitates, primarily in the ferritic phase where the solubility of copper is lower. These precipitates preferentially segregate at grain boundaries, where they transform from fine precipitates to copper-rich phases. Solution annealing can eliminate copper precipitates from austenite, allowing for controlled precipitation during aging. However, the H900 treatment does not meet ASTM hardness standards due to porosity and residual ferrite content, which reduce hardness. Niobium carbides persist at grain boundaries, regardless of the thermal treatment, due to their high thermal stability.

Surface treatment using LEHCEB with higher accelerating voltage (30 kV) results in a thicker martensitic layer with a low average roughness, while a lower voltage (20 kV) produces a thinner and less homogeneous layer, characterized by residual open pores. The treated surface exhibited fine martensitic grains, with δ ferrite largely absent, indicating that rapid cooling after surface fusion prevented the nucleation of ferritic grains.

The surface-treated samples demonstrated superior tribological performance, with a lower and more stable coefficient of friction compared to the as-sintered and H900-treated specimens, as long as the surface layer was not completely consumed. In particular, the 30 kV treated sample showed the best performance, with an extended low-friction region due to the thicker martensitic surface layer. The wear resistance of the surface treated samples improved likely due to the presence of a heat-affected zone beneath the surface, which altered the tribological properties even after the wear of the molten layer. The roughness and the thickness of the treated layer play a critical role in wear behaviour, with the thicker 30 kV layer resulting in minimized wear tracks.

Overall, the findings suggest that the surface can be optimized through careful control of thermal treatments and surface modification processes. However, improvements are needed to meet hardness and wear resistance standards, and further analyses should enlighten the microstructural transformations ongoing during the treatment to identify the strengthening mechanisms along the depth profile.

ACKNOWLEDGEMENTS

The authors acknowledge Gabriele Impellizzeri and Tommaso Tirelli of Aidro srl for the technical and operative support. The authors also acknowledge the team involved in the PASO project, of which this study is a part. The project is funded under the "FONDO PER LA CRESCITA SOSTENIBILE – Bando Accordi Innovazione DM 31/12/21 - DD 18/03/22 - Progetto PASO-Produzione Additiva di Strumentari Ortopedici, B49J23000620005, ID. 10188".

REFERENCES

[1] L COCCHI, M MARIANI, S GRAZIOSI, R VIGANÒ, N LECIS, Design challenges in leveraging binder jetting technology to innovate the medical instrument field, Proc Des Soc. (2024).
[2] W TILLMANN, NF LOPES DIAS, D STANGIER, C SCHAAK, S HÖGES, Heat treatment of binder jet printed 17–4 PH stainless steel for subsequent deposition of tribo-functional diamond-like carbon coatings, Mater Des. (2022).
[3] M YANG, J YAN, P PENG, PD ENRIQUE, MK KESHAVARZ, M VLASEA, Surface functionalization of binder jetted steels through super-solidus liquid phase sintering and electro-spark deposition, Surf Coatings Technol. (2024).
[4] G YELI, MA AUGER, K WILFORD, GDW SMITH, PAJ BAGOT, MP MOODY, Sequential nucleation of phases in a 17-4PH steel: Microstructural characterisation and mechanical properties, Acta Mater. (2017).
[5] CN HSIAO, CS CHIOU, JR YANG, Aging reactions in a 17-4 PH stainless steel, Mater Chem Phys. (2002).
[6] N LECIS, M MARIANI, R BELTRAMI, L EMANUELLI, R CASATI, M VEDANI, ET AL., Effects of process parameters, debinding and sintering on the microstructure of 316L stainless steel produced by binder jetting, Mater Sci Eng A. (2021).
[7] D HUBER, L VOGEL, A FISCHER, The effects of sintering temperature and hold time on densification, mechanical properties and microstructural characteristics of binder jet 3D printed 17-4 PH stainless steel, Addit Manuf. (2021).
[8] M ZAGO, N LECIS, M MARIANI, I CRISTOFOLINI, Analysis of the causes determining dimensional and geometrical errors in 316L and 17-4PH stainless steel parts fabricated by metal binder jetting, Int J Adv Manuf Technol. (2024).
[9] W TILLMANN, NF LOPES DIAS, D STANGIER, C SCHAAK, S HÖGES, Coatability of diamond-like carbon on 316L stainless steel printed by binder jetting, Addit Manuf. (2021).

TORNA ALL'INDICE >